Journal of Power Sources 220 (2012) 108–113

Contents lists available at SciVerse ScienceDirect

Journal of Power Sources

journal homepage: www.elsevier.com/locate/jpowsour

The role of a $TiCl_4$ treatment on the performance of CdS quantum-dot-sensitized solar cells

Jongmin Kim, Hongsik Choi, Changwoo Nahm, Chohui Kim, Seunghoon Nam, Suji Kang, Dae-Ryong Jung, Jae Ik Kim, Joonhyeon Kang, Byungwoo Park*

WCU Hybrid Materials Program, Department of Materials Science and Engineering, Research Institute of Advanced Materials, Seoul National University, Seoul 151-744, Korea

HIGHLIGHTS

- Nanoscale coating enhances the efficiency by ~40% compared with a bare QDSC.
- The main contribution lies in the reduced recombination rate at the interface.
- The amount of CdS sensitizer remains the same with the coating layer.
- Electrolyte diffusion is another factor affecting the performance of QDSCs.

GRAPHICAL ABSTRACT

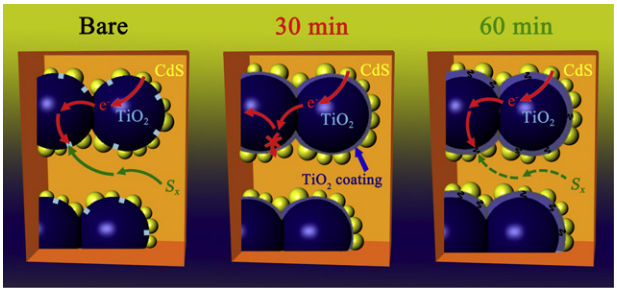

ARTICLE INFO

Article history:
Received 10 May 2012
Received in revised form
5 July 2012
Accepted 31 July 2012
Available online 10 August 2012

Keywords:
Quantum-dot-sensitized solar cells
Cadmium sulfide
Titanium-chloride treatment
Surface passivation
Electrolyte diffusion

ABSTRACT

To investigate the interface of TiO_2/CdS/polysulfide-electrolyte in CdS quantum-dot-sensitized solar cells (QDSCs), a thin TiO_2-coating layer is deposited onto a nanocrystalline TiO_2 electrode by $TiCl_4$. This nanoscale coating enhances the power-conversion efficiency by ~40% compared with a bare CdS-sensitized solar cell. The main contribution to the efficiency enhancement lies in the reduced recombination rate at the TiO_2/polysulfide-electrolyte interface by passivating the surface defects, as confirmed by the open-circuit decay, electrochemical impedance, and chronoamperometry. While the amount of CdS sensitizer remains the same with the coating layer, the optimum coating thickness demonstrates that electrolyte diffusion is another factor affecting the performance of QDSCs.

1. Introduction

Recently, quantum-dot-sensitized solar cells (QDSCs) have received much attention due to their advantages over dye-sensitized solar cells (DSSCs), including higher extinction coefficients of semiconductor nanoparticles compared to dye molecules, the ability to tune the bandgap by changing the nanoparticle size, and the possibility of exceeding the Shockley–Queisser limit by multiple-electron generation [1–5].

Despite these advantages, the efficiency of QDSCs has not reached that of DSSCs [6]. This is due to the large recombination loss at various interfaces in the QDSCs, especially at the TiO_2/quantum-dot/electrolyte interface [7,8]. The excited electrons can be trapped in the defect states within the interface of the TiO_2-electrode/semiconductor/electrolyte, and consequently recombine with holes in the electrolyte redox couple [9]. Moreover, as the optimization of polysulfide electrolyte used in QDSCs has not yet

* Corresponding author. Tel.: +82 2 880 8319; fax: +82 2 885 9671.
E-mail address: byungwoo@snu.ac.kr (B. Park).

0378-7753/$ – see front matter © 2012 Elsevier B.V. All rights reserved.
http://dx.doi.org/10.1016/j.jpowsour.2012.07.133

been achieved, the backward recombination in QDSCs is a more critical issue than in DSSCs [10–13].

For this reason, surface modification is crucial to obtain highly-efficient QDSCs. A TiO_2 layer grown from $TiCl_4$ on a TiO_2-nanoparticle electrode is widely used to improve the conversion efficiency in DSSCs [14–18]. O'Regan's group systematically analyzed the effect of $TiCl_4$ on the performance of DSSCs in terms of injection efficiency, recombination rates, electron-transport rates, and the amount of adsorbed dye molecules. They claimed that both the injection-efficiency enhancement and the reduction of recombination rate were responsible for the increase in conversion efficiency. Nevertheless, the effect of the surface coating by the same TiO_2 materials on reducing the recombination rate has not been fully understood in DSSCs. Moreover, in the case of QDSCs, no reports are available that simultaneously consider the modification of electrolyte diffusivity through the TiO_2 electrode, grain size of TiO_2, charge recombination at the TiO_2/quantum-dot/electrolyte interface, and the amount of semiconductor sensitizer. Therefore, it is essential to systematically investigate the reactions at the electrode interface to identify the mechanisms for both the enhancement and deterioration when TiO_2 coating is incorporated in QDSCs.

2. Experimental procedure

Commercial TiO_2 nanopaste (Ti-Nanoxide D: Solaronix, Switzerland) was used as a host material for QDSCs. The paste was spread by a doctor-blade method on a fluorine-doped tin-oxide (FTO, TEC 8: Pilkington, Japan) electrode, and the paste-coated electrodes were subsequently annealed at 450 °C for 30 min in ambient air. The thickness of the TiO_2-nanoparticle layer was approximately 4 μm, and the active area was 0.28 cm^2.

Post treatment with a 40 mM titanium chloride ($TiCl_4$: Aldrich, St. Louis, U.S.A.) aqueous solution was performed on the sintered TiO_2 films using various immersion times (15 min, 30 min, and 60 min) at 70 °C. After rinsing with deionized (DI) water and subsequent drying, the electrodes were sintered again at 450 °C for 30 min. Following the $TiCl_4$ treatment and subsequent annealing, the successive ionic-layer adsorption and reaction (SILAR) method was used to form the CdS quantum dots onto the bare and $TiCl_4$-treated TiO_2-nanoparticle electrodes. The as-prepared TiO_2 electrodes were immersed in 0.04 M cadmium chloride ($CdCl_2$: Aldrich, St. Louis, U.S.A.) dissolved in methanol for 1 min, and then dipped for another 1 min into 0.04 M sodium sulfide (Na_2S: Aldrich, St. Louis, U.S.A.) in methanol. This process was repeated seven times. A polysulfide solution of 0.5 M Na_2S, 1 M S, and 0.02 M KCl in methanol/water (7/3 vol.%) was used as an electrolyte. Rf-sputtered Au thin film on an FTO substrate was used as a counter electrode for the QDSCs. Thermoplastic foil (25 μm: Dupont, North Carolina, U.S.A.) was used as a spacer for the sandwich-type solar cells.

The nanostructures of the TiO_2 nanoparticles were analyzed by X-ray diffraction (XRD, M18XHF-SRA: McScience, Korea). The photocurrent–voltage (J–V) curves were measured using a solar-cell measurement system (K3000: McScience, Korea) under a solar simulator (Xenon lamp, air mass (AM) 1.5, 100 mW cm^{-2}). An incident photon-to-current conversion efficiency (IPCE) measurement system (K3100: McScience, Korea) was used to obtain the external quantum efficiency. Impedance spectra and open-circuit decay measurements were characterized by a potentiostat (CHI 608C: CH Instrumental Inc., Austin, U.S.A.) and a solar simulator (PEC-L11: Peccell, Japan) under AM 1.5 illumination at open-circuit voltage. The electrochemical impedance spectra were recorded over a frequency range from 10^{-1} to 10^5 Hz. The cyclic voltammetry was measured by an electrochemical analyzer (CHI 604A: CH Instrumental Inc., Austin, U.S.A.). An inductively coupled plasma-atomic emission spectrometer (ICP-AES, Optima-4300 DV: Perkin–Elmer, MA, U.S.A.) was used to determine the ratio of Cd/Ti in the electrode.

3. Results and discussion

Fig. 1 shows the J–V curves of the CdS-sensitized solar cells as a function of $TiCl_4$-treatment time. Improvements in the open-circuit voltage, short-circuit current, and power-conversion efficiency are observed as the treatment time increases (Table 1). On the other hand, after 60-min treatment, both the fill factor and cell efficiency decrease, indicating the existence of an optimum TiO_2-coating layer thickness for QDSCs.

To attain the optimum solar-cell performance, several factors need to be considered: the charge-recombination rate from the TiO_2 conduction band to the electrolyte at the TiO_2/CdS/polysulfide interface, electrolyte diffusion through the porous TiO_2 matrix, and the amount of CdS quantum dots [19]. The open-circuit voltage is mainly affected by the TiO_2 conduction-band position, and recombination rates [20,21], and the short-circuit current is influenced by the light-harvesting efficiency, recombination rates, and transport properties [22,23].

To investigate the change of the TiO_2 host material after $TiCl_4$ treatment, XRD analysis was performed. The diffraction pattern shows pure anatase phase, with no secondary phases, as is shown in Fig. 2. The CdS phase is identified as the wurtzite phase (not shown here). The grain size of the TiO_2 nanoparticles was calculated from the Scherrer equation of Δk vs. k (the scattering vector $k = (4\pi\lambda^{-1})\sin\theta$). The five peaks were fitted using a double-peak Lorentzian function for $K\alpha_1$ and $K\alpha_2$ [24,25]. The grain size gradually increases with the increase of the $TiCl_4$-treatment time, which is consistent with the mass change of TiO_2 after the treatment (9%, 27%, and 35%). This indicates that the TiO_2 layer grown from $TiCl_4$ remains the same anatase phase, and the suppression of electron recombination is not caused by the passivation of a different phase (rutile or amorphous phase). The residual local strain (in the parentheses of Fig. 2) is reduced after the $TiCl_4$ treatment (despite the large error bar), indicating the possibility of defect reduction at the surface of TiO_2 nanoparticles.

Various types of defects can exist at the surface of TiO_2, such as oxygen vacancy, hydroxyl group, bridge-bonded oxygen, fivefold coordinated Ti atoms, etc. [26,27]. The suppression of defect-related photoluminescence by the TiO_2-coating layer has been reported by several groups [28,29]. Other groups' work have shown

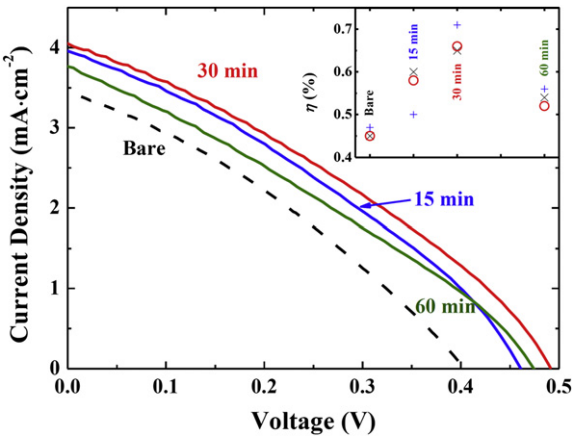

Fig. 1. Photocurrent–voltage curves of CdS quantum-dot-sensitized solar cells with various TiO_2-coating times. The inset shows power-conversion efficiency of QDSCs as a function of the coating time.

Table 1
Short-circuit current (J_{sc}), open-circuit voltage (V_{oc}), fill factor (*FF*), and power-conversion efficiency (η) of the QDSCs with and without $TiCl_4$ treatment.

	J_{sc} (mA cm^{-2})	V_{oc} (V)	*FF*	η
Bare	3.44	0.400	32.7%	0.45%
15 min	3.98	0.461	32.8%	0.60%
30 min	4.05	0.492	32.7%	0.65%
60 min	3.76	0.474	30.3%	0.54%

that the growth of TiO_2 from gaseous $TiCl_4$ is initiated at the surface states such as oxygen vacancies or dangling bonds [30,31]. Similar mechanisms may be possible when the solution process is used because of the high interfacial free energy along the defect sites. Moreover, the increase in local strain with the $TiCl_4$-treatment time (Fig. 2) indicates that residual strain exists in the coating layer, because of the volume change (~130%) during the formation of the TiO_2-coating layer from titanium hydroxide [32].

The IPCE is a useful tool for analyzing light-harvesting efficiency because the spectral response would be changed with the quantity of sensitizer [33]. As shown in Fig. 3, symmetric increase of IPCE is observed after TiO_2 coating. Therefore, efficiency enhancement is not caused by the light-harvesting efficiency of the CdS sensitizer. From ICP-AES, the Cd/Ti atomic ratios were 0.18, 0.19, 0.18, and 0.19, respectively, for the bare, 15-min, 30-min, and 60-min $TiCl_4$-treated samples (The Ti mass is normalized to the original mass before the $TiCl_4$ treatment). This result also shows that the amount of CdS sensitizer in the $TiCl_4$-treated electrode is almost the same as that for the bare sample.

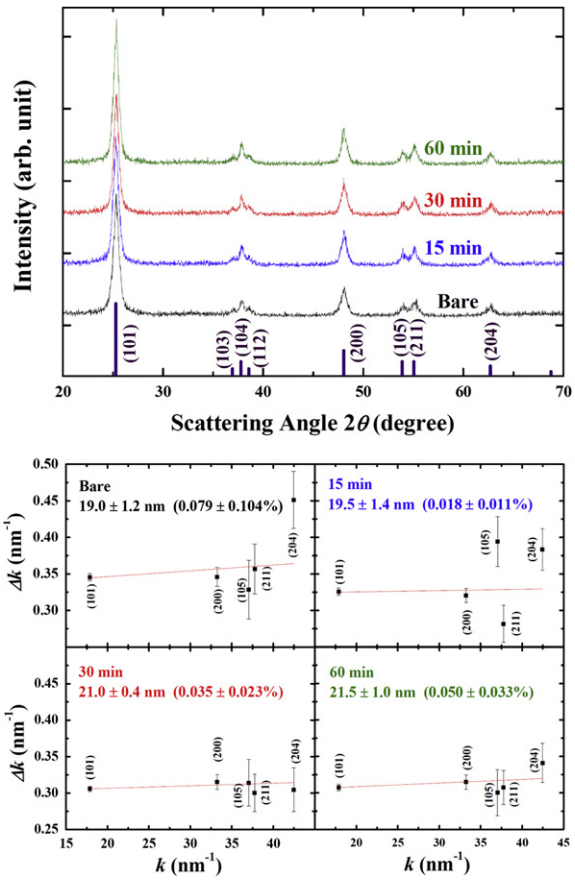

Fig. 2. X-ray diffraction of the bare and $TiCl_4$-treated nanocrystalline film to determine the grain size and local strain of TiO_2 nanocrystals from the Δk vs. k plot.

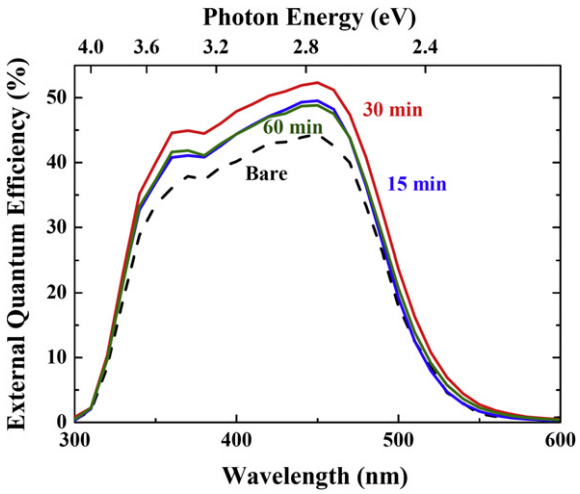

Fig. 3. Incident photon-to-current conversion efficiency (IPCE) spectra of CdS-QDSCs with various $TiCl_4$-treatment conditions.

The junction characteristics were examined by dark-current measurements (Fig. 4) [34,35]. With the TiO_2 coating, the dark current shows enhanced junction characteristics with a small leakage current, which means that the back-electron transfer from the TiO_2-nanoparticle layer to the polysulfide electrolyte is effectively blocked by the coating layer. In the sensitized solar cell, the surface recombination and electrolyte diffusion are connected in series [36]. The dark current depends on the recombination at the interface of TiO_2/electrolyte ($R_{recom} >> R_{diff}$) in the low-voltage region. On the other hand, in the high-voltage region, due to the high flux of electrons and large driving force for recombination, diffusion resistance of electrolyte determines the current ($R_{recom} << R_{diff}$) [36]. Therefore, the dark current should be analyzed considering these two factors. In the case of 60-min-treated cell, the leakage current in the low-voltage region exhibits slightly higher value than that of the 30-min-treated cell, which is consistent with other experiments (in the following Fig. 5 for electrochemical impedance, Fig. 6 for electron lifetime, and Fig. 7 for chronoamperometry). On the other hand, the slope of current density in the high-voltage region is smaller than that of the 30-min-treated cell, indicating higher series resistance by 60-min treatment [37].

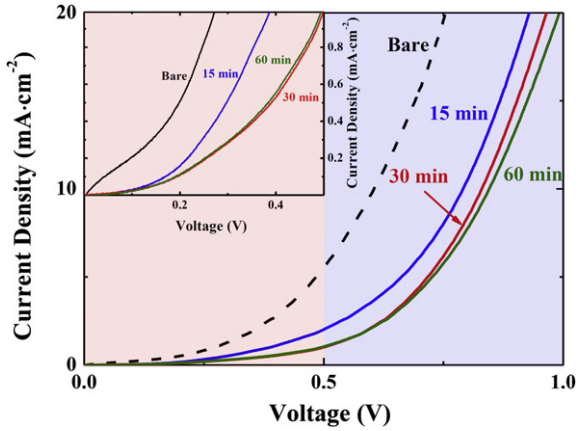

Fig. 4. Dark current of the bare and TiO_2-coated CdS-sensitized solar cells with various coating times. The inset shows magnified dark current in the low-voltage region.

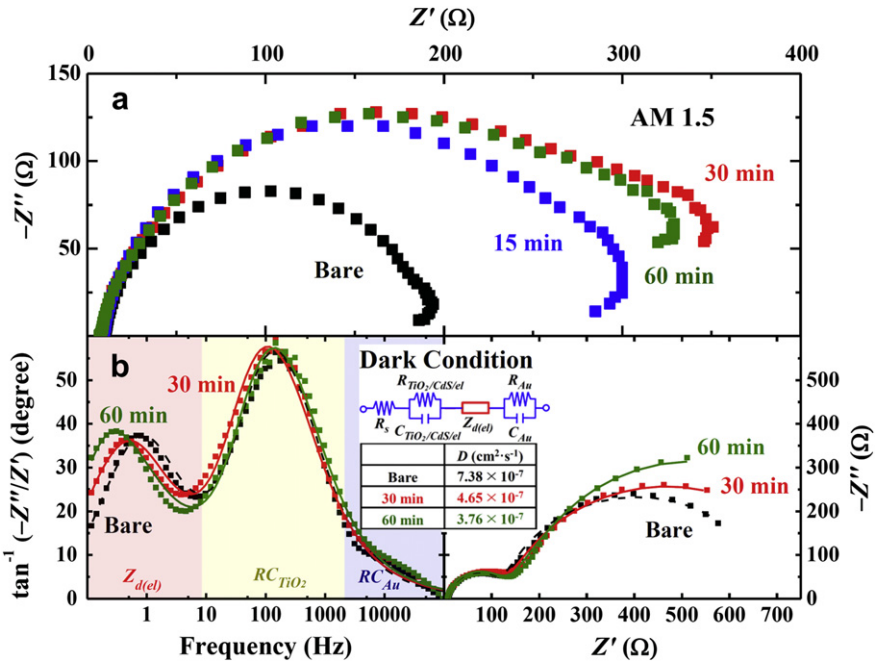

Fig. 5. (a) Electrochemical impedance spectra measured under AM 1.5 illumination, and (b) Bode and Nyquist plots measured under dark conditions with various $TiCl_4$-treatment conditions at V_{oc}.

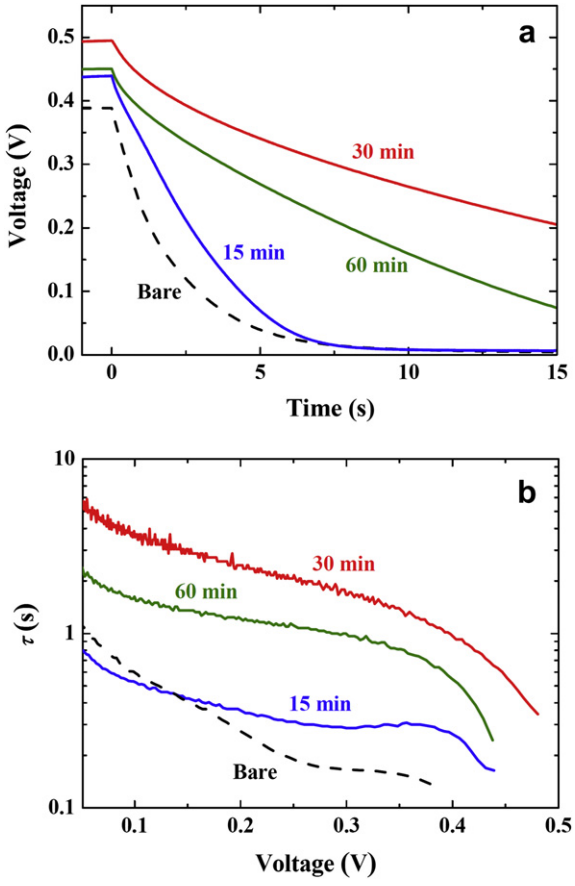

Fig. 6. (a) Experimental decay results of open-circuit voltage for the CdS-sensitized solar cells with various $TiCl_4$-treatment conditions. (b) Electron lifetimes as a function of voltage.

The charge-transfer kinetics at the TiO_2/CdS/polysulfide-electrolyte interface were investigated by impedance analysis at the open-circuit voltage under AM 1.5 illumination. As shown in Fig. 5(a), the charge-transfer resistance shows higher values with increasing time of $TiCl_4$ treatment, which means that the TiO_2-coating layer effectively suppresses charge transfer at the TiO_2/CdS/electrolyte interface. It is interesting that hook-like inductive characteristics at lower frequency are observed in all of the samples. This inductive feature is associated with the inefficient diffusion of polysulfide electrolyte which accelerates the recombination between electrons in TiO_2 nanoparticles and holes in electrolyte under illumination [38,39].

Since no net current flows through the cell under illumination at V_{oc}, the impedance was also measured without illumination at the open-circuit voltage (dark condition) to obtain the diffusivity of

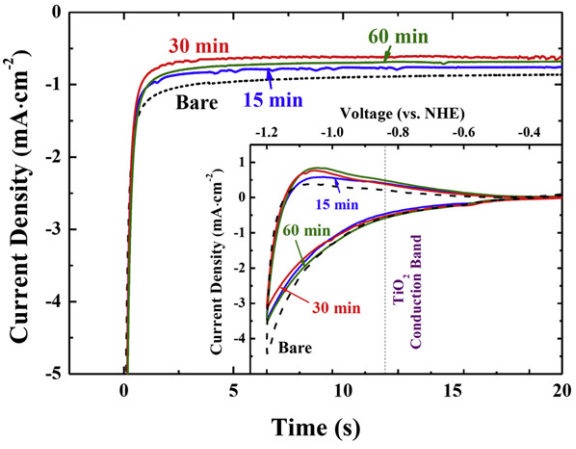

Fig. 7. Chronoamperometry of reduction current from bare and $TiCl_4$-treated TiO_2-nanoparticle film measured at −1.1 V vs. NHE in the polysulfide electrolyte. The inset shows cyclic voltammetric curves of the bare and $TiCl_4$-treated TiO_2-nanoparticle electrode. The TiO_2 conduction-band position is illustrated as a short-dashed line.

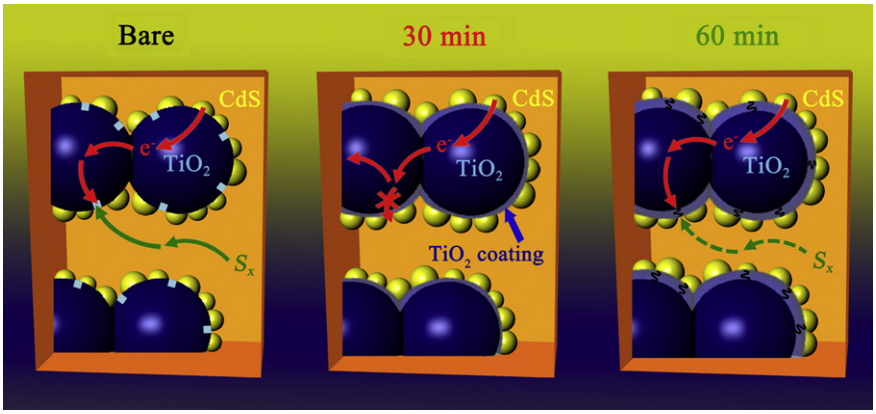

Fig. 8. Schematic figures of the $TiCl_4$-treatment effects on the performance of CdS-sensitized solar cells.

polysulfide electrolyte through the porous TiO_2 electrode (Fig. 5(b)) [40–42]. The three semicircles (reduction at the counter electrode, recombination at the TiO_2/electrolyte interface, and diffusion of electrolyte) can be easily identified because each reaction has its characteristic frequency range, as shown in the Bode plot of Fig. 5(b) [37,43]. Because TiO_2 becomes sufficiently conductive at V_{oc} [44], and the first semicircle at high frequency from the Au counter electrode is large enough to hide electron-transport (Warburg) behavior [33], we can ignore the electron-transport resistance through nanoparticles, allowing the equivalent circuit to be slightly simplified (inset of Fig. 5(b)) [45,46]. The electrolyte diffusivity in the low-frequency range (0.1–1 Hz), and the corresponding diffusion coefficient decreased with the amount of TiO_2 coating. The fitting lines are shown as solid/dashed lines in Fig. 5(b). The amount of TiO_2 coating onto the nanoparticle electrode scales with the $TiCl_4$-treatment time. As a result, the pore size within TiO_2-nanoparticle film decreases. Furthermore, the diffusivity of polysulfide electrolyte without TiO_2 nanoparticles ($\sim 10^{-6}$ cm^2 s^{-1}) is approximately 2 orders of magnitude lower than that of the iodide electrolyte used in the DSSCs ($\sim 10^{-4}$ cm^2 s^{-1}) [47,48], and the size of the semiconductor sensitizer (2–6 nm) is larger than that of a dye molecule ($\sim$1 nm) [49]. Therefore, the electrolyte diffusion through the nanopore is inevitably difficult. This result is consistent with the dark-current experiment (Fig. 4), and the increase of series resistance at V_{oc} (from the slope) for the 60-min-coated cell (Fig. 1).

Since the impedance results depend on the sum of reaction characteristics in QDSCs (electron transport, charge transfer, electrolyte diffusion, etc.), an additional photovoltage-decay measurement was performed to separate out the recombination behavior at the TiO_2/CdS/electrolyte interface from other reactions (Fig. 6), and the corresponding decay time was calculated using a simple equation [12]. The decay rate becomes slow, and the corresponding electron lifetime increases with $TiCl_4$ treatment, which indicates that more electrons are accumulated in the TiO_2 electrode due to the reduced recombination at the TiO_2/CdS/electrolyte interface [50].

To further characterize the recombination behavior at the TiO_2/polysulfide interface, chronoamperometry measurement was performed at a voltage of −1.1 V vs. NHE (above the TiO_2 conduction band), from −0.4 V vs. NHE (within the bandgap of TiO_2). With the TiO_2-nanoparticle electrode as the working electrode, a Pt wire and a Ag/AgCl electrode were used as counter and reference electrodes, respectively, in the polysulfide electrolyte. As shown in the chronoamperometry of Fig. 7, the $TiCl_4$-treated sample displays smaller reduction current than the bare TiO_2 sample, and shows an increase with a thicker TiO_2-coating layer, consistent with other analyses. Cyclic voltammetry is another tool for analyzing the electrolyte oxidation/reduction reaction at the semiconductor interface. The continuous reduction current of injected electrons from the TiO_2 nanoparticles to the polysulfide electrolyte is suppressed by the $TiCl_4$ treatment (inset of Fig. 7) [52]. The oxidation peak of TiO_2 valence band ($\sim$2.4 V vs. NHE) is not observed because it is not in the range of interest. The approximate conduction-band position of the TiO_2 film was calculated from the pH value of the electrolyte, and the TiO_2 conduction-band position at pH 0. The onset potential of reduction current (approximately −0.8 V vs. NHE), which is similar to the conduction band of TiO_2, is maintained in spite of the TiO_2 coating on the TiO_2 electrode. This means that the conduction-band position is not significantly altered by the coating layer [51].

All of the above results show that the reduced recombination at the TiO_2/electrolyte interface is the main reason for the enhancement of conversion efficiency. The proposed mechanism is that the growth of the TiO_2-coating layer is initiated at the defects or dangling bonds of the host TiO_2 material. As a result, the coating layer passivates the surface defects, and suppresses the recombination at the TiO_2/electrolyte interface. Furthermore, correct TiO_2 coating can decrease the trap states within the TiO_2/CdS interface in QDSCs. On the other hand, when the coating layer becomes too thick, the large volume change during the $TiCl_4$ hydrolysis induces residual strain in the coating layer so that the recombination increases again. Moreover, a thick coating layer impedes the polysulfide diffusion through the porous TiO_2 electrode.

Fig. 8 shows a schematic illustration for the effect of the TiO_2-coating layer. The electron recombination at the interface of TiO_2/CdS/polysulfide-electrolyte is suppressed by the $TiCl_4$-treated coating layer. As a result, the number of electrons captured by the FTO electrode increases (increase of J_{sc}), and the electron accumulation in the TiO_2 layer is improved by reduced recombination (increase of V_{oc}), therefore the power-conversion efficiency is enhanced. On the other hand, the coating layer eventually increases both the residual strain of the TiO_2 nanoparticles and the series resistance of the electrolyte. Thus, the fill factor and cell efficiency decrease with comparatively-thick coating layers.

4. Conclusions

The effect of TiO_2-coating layer is systematically analyzed considering the factors affecting the QDSC's performance. The enhanced efficiency by the nanoscale coating on the TiO_2 electrode is attributed to the reduction of detrimental recombination at the TiO_2/CdS/polysulfide-electrolyte interfaces by passivating the surface defects present on the TiO_2-nanoparticle layer, as has been confirmed by various analyses, while the amount of CdS sensitizer

remains the same with $TiCl_4$ treatment. Also, as distinct from DSSCs, electrolyte diffusion into the porous nanoparticle layer can be one of the reasons for the diminishing efficiency of QDSCs due to the low diffusivity of polysulfide electrolyte and large size of the semiconductor sensitizers than that of the dye molecules.

Acknowledgments

This research was supported by the National Research Foundation of Korea, through the World Class University (WCU, R31-2008-000-10075-0) and the Korean Government (MEST:NRF, 2010-0029065).

References

[1] P.V. Kamat, K. Tvrdy, D.R. Baker, J.G. Radic, Chem. Rev. 110 (2010) 6664–6688.
[2] W. Yu, X. Peng, Angew. Chem. Int. Ed. 41 (2002) 2368–2371.
[3] R.J. Ellingson, M.C. Beard, J.C. Johnson, P. Yu, O.I. Micic, A.J. Nozik, A. Shabaev, A.L. Efros, Nano Lett. 5 (2005) 865–871.
[4] J.B. Sambur, T. Novet, B.A. Parkinson, Science 330 (2010) 63–66.
[5] O.E. Semonin, J.M. Luther, S. Choi, H.-Y. Chen, J. Gao, A.J. Nozik, M.C. Beard, Science 334 (2011) 1530–1533.
[6] Q. Zhang, X. Guo, X. Huang, S. Huang, D. Li, Y. Luo, Q. Shen, T. Toyoda, Q. Meng, Phys. Chem. Chem. Phys. 13 (2011) 4659–4667.
[7] I. Mora-Seró, J. Bisquert, J. Phys. Chem. Lett. 1 (2010) 3046–3052.
[8] I. Mora-Seró, S. Gimenez, F. Fabregat-Santiago, R. Gomez, Q. Shen, T. Toyoda, J. Bisquert, Acc. Chem. Res. 42 (2009) 1848–1857.
[9] G. Hodes, J. Phys. Chem. C 112 (2008) 17778–17787.
[10] Z. Yang, C.-Y. Chen, C.-W. Liu, H.-T. Chang, Chem. Commun. 46 (2010) 5485–5487.
[11] P. Ardalan, T.P. Brennan, H.-B.-R. Lee, J.R. Bakke, I.-K. Ding, M.D. McGehee, S.F. Bent, ACS Nano 5 (2011) 1495–1504.
[12] J. Kim, H. Choi, C. Nahm, J. Moon, C. Kim, S. Nam, D.-R. Jung, B. Park, J. Power Sources 196 (2011) 10526–10531.
[13] J.-Y. Hwang, S.-A. Lee, Y.H. Lee, S.-I. Seok, Appl. Mater. Interfaces 2 (2010) 1343–1348.
[14] N. Fuke, R. Katoh, A. Islam, M. Kasuya, A. Furube, A. Fukui, Y. Chiba, R. Komiya, R. Yamanaka, L. Han, H. Harima, Energy Environ. Sci. 2 (2009) 1205–1209.
[15] S. Ito, P. Liska, P. Comte, R. Charvet, P. Pechy, U. Bach, L.S. Mende, S.M. Zakeeruddin, A. Kay, M.K. Nazeeruddin, M. Grätzel, Chem. Commun. (2005) 4351–4353.
[16] P.M. Sommeling, B.C. O'Regan, R.R. Haswell, H.J.P. Smit, N.J. Bakker, J.J.T. Smits, J.M. Kroon, J.A.M. van Roosmalen, J. Phys. Chem. B 110 (2006) 19191–19197.
[17] B.C. O'Regan, J.R. Durrant, P.M. Sommeling, N.J. Bakker, J. Phys. Chem. C 111 (2007) 14001–14010.
[18] P.R.F. Barnes, A.Y. Anderson, S.E. Koops, J.R. Durrant, B.C. O'Regan, J. Phys. Chem. C 113 (2009) 1126–1136.
[19] P. Tiwana, P. Parkinson, M.B. Johnston, H.J. Snaith, L.M. Herz, J. Phys. Chem. C 114 (2010) 1365–1371.
[20] C.-H. Lin, S. Chattopadhyay, C.-W. Hsu, M.-H. Wu, W.-C. Chen, C.-T. Wu, S.-C. Tseng, J.-S. Hwang, J.-H. Lee, C.-W. Chen, C.-H. Chen, L.-C. Chen, K.-H. Chen, Adv. Mater. 21 (2009) 759–763.
[21] L. Larina, D. Shin, J.H. Kim, B.T. Ahn, Energy Environ. Sci. 4 (2011) 3487–3493.
[22] C. Nahm, H. Choi, J. Kim, D.-R. Jung, C. Kim, J. Moon, B. Lee, B. Park, Appl. Phys. Lett. 99 (2011) 253107.
[23] A. Mihi, C. Zhang, P.V. Braun, Angew. Chem. Int. Ed. 50 (2011) 5712–5715.
[24] D.-R. Jung, D. Son, J. Kim, C. Kim, B. Park, Appl. Phys. Lett. 93 (2008) 163188.
[25] D. Son, D.-R. Jung, J. Kim, T. Moon, C. Kim, B. Park, Appl. Phys. Lett. 90 (2007) 101910.
[26] S. Wendt, P.T. Sprunger, E. Lira, G.K.H. Madsen, Z. Li, J.Ø. Hansen, J. Matthiesen, A. Blekinge-Rasmussen, E. Lægsgaard, B. Hammer, F. Besenbacher, Science 320 (2008) 1755–1759.
[27] S.M. Prokes, J.L. Gole, X.B. Chen, C. Burda, W.E. Carlos, Adv. Funct. Mater. 15 (2005) 161–167.
[28] F.J. Knorr, D. Zhang, J.L. McHale, Langmuir 23 (2007) 8686–8690.
[29] H.O. Seo, S.-Y. Park, W.H. Shim, K.-D. Kim, K.H. Lee, M.Y. Jo, J.H. Kim, E. Lee, D.-W. Kim, Y.D. Kim, D.C. Lim, J. Phys. Chem. C 115 (2011) 21517–21520.
[30] X.-S. Wang, X.-W. Guo, Catal. Today 51 (1999) 177–186.
[31] S. Wang, Q. Yang, Z. Wu, M. Li, J. Lu, Z. Tan, C. Li, J. Mol. Catal. A 172 (2011) 219–225.
[32] P.C.A. Alberius, K.L. Frindell, R.C. Hayward, E.J. Kramer, G.D. Stucky, B.F. Chmelka, Chem. Mater. 14 (2002) 3284–3294.
[33] V. González-Pedro, X. Xu, I. Mora-Seró, J. Bisquert, ACS Nano 4 (2010) 5783–5790.
[34] S.W. Boettcher, E.L. Warren, M.C. Putnam, E.A. Santori, D. Turner-Evans, M.D. Kelzenberg, M.G. Walter, J.R. McKone, B.S. Brunschwig, H.A. Atwater, N.S. Lewis, J. Am. Chem. Soc. 133 (2011) 1216–1219.
[35] T. Moon, J.H. Jun, H. Lee, W. Yoon, S. Kim, B.-K. Lee, H.-C. Lee, W. Kim, S.-H. Ahn, S. Lee, H.-M. Lee, Prog. Photovolt: Res. Appl. 20 (2012) 294–297.
[36] F. Fabregat-Santiago, J. Bisquert, E. Palomares, L. Otero, D. Kuang, S.M. Zakeeruddin, M. Grätzel, J. Phys. Chem. C 111 (2007) 6550–6560.
[37] R. Kern, R. Sastrawan, J. Ferber, R. Stangl, J. Luther, Electrochim. Acta 47 (2002) 4213–4225.
[38] G. Kron, T. Egerter, J.H. Werner, U. Rau, J. Phys. Chem. B 107 (2003) 3556–3564.
[39] I. Mora-Seró, J. Bisquert, F. Fabregat-Santiago, G. Garcia-Belmonte, G. Zoppi, K. Durose, Y. Proskuryakov, I. Oja, A. Belaidi, T. Dittrich, R. Tena-Zaera, A. Katty, C. Lévy-Clément, V. Barrioz, S.J.C. Irvine, Nano Lett. 6 (2006) 640–650.
[40] Q. Wang, J.-E. Moser, M. Grätzel, J. Phys. Chem. B 109 (2005) 14945–14953.
[41] K. Zhu, S.-R. Jang, A.J. Frank, J. Phys. Chem. Lett. 2 (2011) 1070–1076.
[42] H. Choi, C. Nahm, J. Kim, J. Moon, S. Nam, C. Kim, D.-R. Jung, B. Park, Curr. Appl. Phys. 12 (2012) 737–741.
[43] T. Hoshikawa, M. Yamada, R. Kikuchi, K. Eguchi, J. Electrochem. Soc. 152 (2) (2005) E68–E73.
[44] F. Fabregat-Santiago, J. Bisquert, G. Garcia-Belmonte, G. Boschloo, A. Hagfeldt, Sol. Energy Mater. Sol. Cells 87 (2005) 117–131.
[45] S.-H. Anna Lee, A.-M.S. Jackson, A. Hess, S.-T. Fei, S.M. Pursel, J. Basham, C.A. Grimes, M.W. Horn, H.R. Allcock, T.E. Mallouk, J. Phys. Chem. C 114 (2010) 15234–15242.
[46] V. Yong, S.-T. Ho, R.P. Chang, Appl. Phys. Lett. 92 (2008) 143506.
[47] G. Kron, U. Rau, M. Dürr, T. Miteva, G. Nelles, A. Yasuda, J.H. Werner, Electrochem. Solid-State Lett. 6 (2003) E11–E14.
[48] R. Zito, Energy Storage: A New Approach, Scrivener Publishing, MA, 2010.
[49] T. Miyasaka, J. Phys. Chem. Lett. 2 (2011) 262–269.
[50] A. Zaban, M. Greenshtein, J. Bisquert, ChemPhysChem 11 (2010) 2290–2304.
[51] Z. Zhang, S.M. Zakeeruddin, B. O'Regan, R. Humphry-Baker, M. Grätzel, J. Phys. Chem. B 109 (2005) 21818–21824.
[52] N. Guijarro, J.M. Campinã, Q. Shen, T. Toyoda, T. Lana-Villarreal, R. Gómez, Phys. Chem. Chem. Phys. 13 (2011) 12024–12032.